Acta Materialia Transylvanica 8/2. (2025) 105–112.
DOI: Hungarian: https://doi.org/10.33923/amt-2025-02-10
English: https://doi.org/10.33924/amt-2025-02-10

Simulation Analysis of Internal Stresses in Implant Screws

Ádám VÖRÖS,[1] Csanád PESKE,[2] Klaudia TALABÉRNÉ KULCSÁR [3]

[1] *Széchenyi István University, Audi Hungaria Faculty of Automotive Engineering, Department of Materials Science and Machine Design, Győr, Hungary, voros.adam@hotmail.com*

[2] *Óbuda University Alba Regia Faculty, Institute of Engineering. Székesfehérvár, Hungary, peskecsanad@gmail.com*

[3] *Óbuda University Alba Regia Faculty, Institute of Engineering. Székesfehérvár, Hungary, kulcsar.klaudia@amk.uni-obuda.hu*

Abstract

The aim of this study was to investigate the failure of titanium alloy fixation screws (connecting the implant and the abutment) used in custom-made subperiosteal implants. Once the cause of failure was determined, our main objective was to determine the maximum tightening torque for the existing design. To achieve this, 3D CAD screw models were examined using finite element software. Based on the results obtained, we were able to recommend a tightening torque interval to the screw manufacturer that was guaranteed not to lead to failure (provided that the screws are manufactured according to the dimensional tolerances specified in the drawing). Our secondary objective was to improve the design of the screw to ensure that the failure could be fully eliminated. In this paper we will describe the failure mode, its cause, the methodology of our investigation, the results obtained, the conclusions drawn and finally, future research opportunities.

Keywords: *subperiosteal implant, screw joint, simulation, finite element analysis.*

1. Introduction

Finite Element Method is a state-of-the-art numerical method, which is widely used in the simulation and analysis of physical phenomena. This method enables the optimization of components for more efficient and cost-effective product development [1]. In the field of medicine, especially in dentistry, numerical analysis has become an indispensable tool for the study of complex biomechanical systems that are difficult or impossible to analyse in vivo or in vitro [2, 3].

In the design and evaluation of dental implants, numerical analysis allows a detailed assessment of the stability and reliability of the interface between the implant and the surrounding bone. Overloading or underloading can have a significant impact on bone loss, which highlights the importance of accurately modelling the biomechanical behaviour of implant [5]. The application of the method also includes the analysis of dynamic and fatigue loads, which are key to predicting the long-term success of implants [3, 4].

Biomechanical optimisation plays a key role in the design of dental implants. Finite element method allows us to evaluate the effects of different implant designs and to fine-tune design parameters for long-term stability [1, 2]. In addition, finite element method allows to consider the effect of friction on screw preload, which is a critical factor for the durability of prosthetic structures [4, 6].

Overall, numerical modelling enables a comprehensive understanding of the complex biomechanical behaviour of dental implants. It contributes to improved clinical outcomes and reduced prosthetic complications [7, 8].

2. The need for analysis

2.1. Subperiosteal implants

Modern dental implants used today can be divided into three main types. The most used type is endosteal implants, which are usually screw threaded implants that are placed directly into the jawbone. If the bone volume does not allow

the use of screw implants, transosteal implants (implants that are placed through and fixed to the jawbone) or subperiosteal implants (implants that are placed over and fixed to the mandible or maxilla) may be used. The main components of subperiosteal implants are shown in Fig. 1. [9, 10].

The framework base is usually created with additive manufacturing from Ti-6Al-4V powder. After manufacturing, the piece is post-processed on a 5-axis milling machine to form the threads and the surfaces that would incorporate the interfaces (sleeves). The interfaces (which will later receive the crown or denture superstructure) and the fixation screws are usually made of Ti-6Al-4V ELI based titanium alloy, machined (turning) from bar stock.

In this study, we investigated the screws used to fix the implant framework to the interface in subperiosteal implants. Fig. 2. shows a technical drawing of an implant screw with its main dimensions and tolerances.

2.2. Problem statement

As can be seen in Fig. 2. the screws used have M1.8 threads. To tighten these and similar sized screws, dentists usually use a tightening torque of 255 Ncm.

To tighten the screw, the internal keyhole slot with a 1.3 mm flat width is used. To maintain the torque interval, a calibrated torque wrench is used. A bit head provides the connection between the screwdriver and the screw. To ensure that the screws can be tightened with as high torque as possible without damaging the internal keyhole or bit head, the size of the keyhole opening must be maximised. The size of the screw head is limited due to space constraints, and the total length protruding from the upper plane of the receiving (nut) thread must not be greater than Ø2,4 × 2,2 mm as shown in the drawing.

For this reason, the design and dimensions of the internal keyway must be carefully selected to avoid leaving too small a wall thickness between the outer surface of the screw head or the undercut required by the thread runout and the internal keyway or its pilot hole. The surfaces connected by these potential fracture lines are illustrated in four different cross-sections for improved clarity and are marked in pairs using different colors, as well as with the labels a, b, and c in Fig. 3. If not properly selected, the stresses arising in the screw head may exceed the yield strength of the screw material (795 N/mm²), causing shear fail-

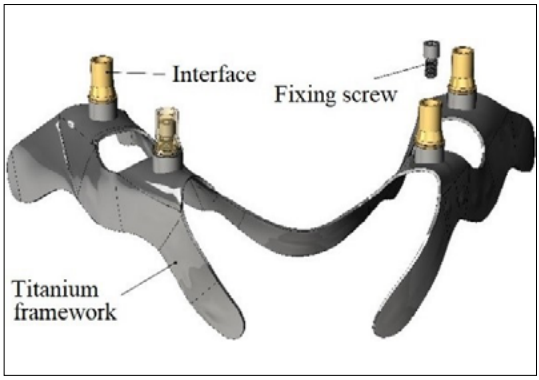

Fig. 1. *Main components of subperiosteal implants.*

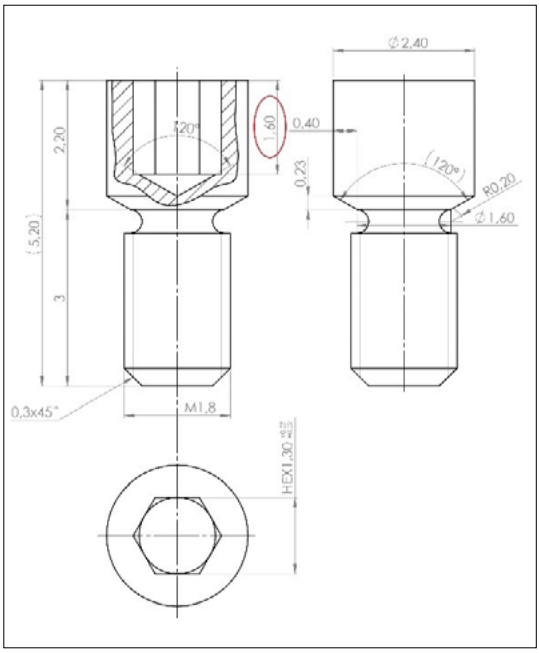

Fig. 2. *Technical drawing of interface fixing screw with its main dimensions.*

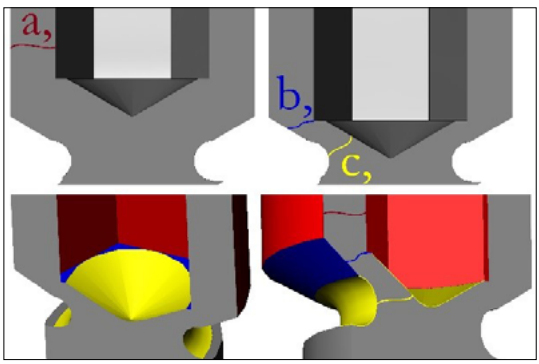

Fig. 3. *Critical cross-sections.*

ure between the screw head and the shank (screw head breaking off). [9].

Based on the location of the narrowest cross-section, three different critical cross-sections can be distinguished, the locations of which are shown in Fig. 3.

In case a, the fracture occurs between one tip of the hexagon and the side of the screw head. In this case, this is not relevant, as the size of the key is carefully selected and repeatedly checked. Moreover, it cannot be modified. In case b, the fracture occurs between the tapered part of the screw head and the gap. In case c, the fracture occurs between the tip of the technological (pilot) hole of the internal keyhole and the undercut required by the thread run-out.

The latter two are due to the choice of a keyhole opening that is too deep. Fig. 4. shows a screw after failure. In this case, the fracture occurred in cross-section c.

The reason for our research is that during the assembly of a sample prepared for load testing, some screws sheared at as little as 30 Ncm.

In this preliminary study, we examined a total of four different screws, all of which were individually machined on a lathe. Failure occurred at 30 Ncm, 32.6 Ncm, 33 Ncm, and 55 Ncm, respectively. Since the result at 55 Ncm differs by ~20 Ncm from the other torque values, we suspect a one-off manufacturing defect in the other screws.

Fig. 5. shows the torque wrench used in the mentioned study, specifically the Stahlwille Torsiotronic 1.2 model.

It is important to note, however, that due to the multiple testing prior to clinical use and the strict quality management systems in place, no production defective screw can be supplied to the end-user. At the same time, the aim is to ensure that screws that could fail under such load in the future are not produced in the first place.

Basically, for the internal keyway of the screws, the pilot hole can have 3 different vertex angles. These angles are defined by that of the selected pilot drills. Out of these three versions, we have considered the two most common cases of 180° and 120° pilot drills, but there are also 140° drills available. The vertex angles of the pilot drills and their corresponding hole patterns (in ascending order from left to right according to the size of the tip angle) can be observed in Fig. 6.

3. CAD model description

In this paper, a simulation study of the internal stresses within implant screws was performed. The model is shown in Fig. 7.

Fig. 4. *Ccrew after failure, two broken-off screw heads and one threaded shaft.*

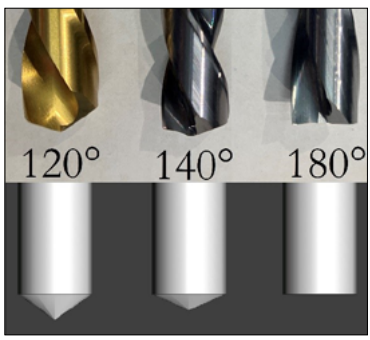

Fig.6. *Vertex angle options for pilot drills and their respective pilot hole geometries.*

Fig. 5. *Utilized torque wrench*

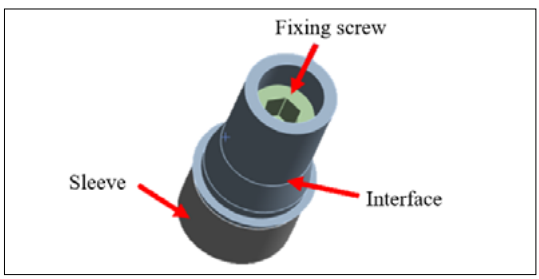

Fig. 7. *The CAD modell.*

The model was made up of 3 parts: the sleeve material was Ti-6Al-4V (Grade 5), which was manufactured using additive manufacturing together with the subperiosteal implant. The model also included the interface and the screw, which were both made of Ti-6Al-4V ELI (Grade 23) titanium alloy. The screw and the sleeve did not contain threads, they were created by post-geometric transformation in the simulation software. Ansys (engineering simulation software) considers all contact surfaces as „bonded" after importing them. It means that no displacement is allowed between the components. The bonds between the parts had to be manually adjusted: the connection between the sleeve and the interface remained „bonded", the connection between the sleeve and the screw was „frictional", and the connection between the interface and the screw was selected to be „rough", which allows the elements to separate. As the sleeve and the implant are created together, fixed connection was considered between them. The implant osseointegrates and can therefore move together with the jaw. The load was defined as the screw tightening torque, with values between 10 Ncm and 80 Ncm. The selected boundary conditions are shown in **Fig. 8** .

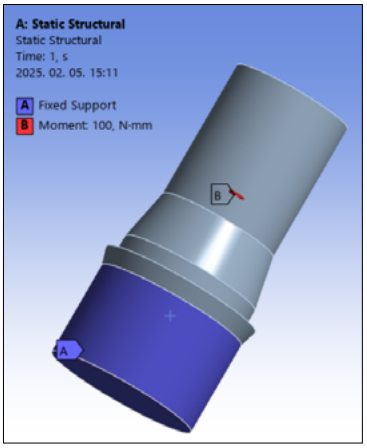

Fig. 8. *CAD-model and boundary conditions.*

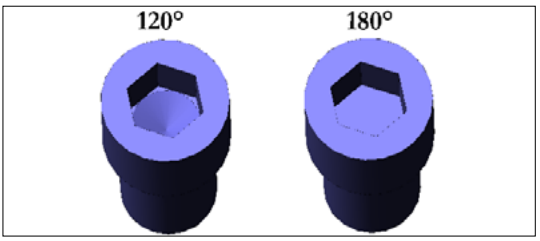

Fig. 9. *Designs of different vertex angles.*

4. Analyses

Our tests were carried out on two types of fixing screws: one with a 120-degree and one with a 180-degree tip angle. These are shown in **Fig. 9**.

Tetrahedral meshing technique was selected. In the case of the 120° vertex angle, the number of nodes ranged from 51 260 to 53 194. The element numbers were between 33 289 – 34 776. For the 180° vertex angle, these values were as follows: the number of nodes ranged from 51 447 – 52 566 and the element numbers ranged from 33 455 – 34 325. Denser meshing was applied for the study area.

5. Results of numerical analyses

In this paper, the stresses arising in the screw at the thread runout groove and at the thread were analysed. Based on the results, it can be stated that the maximum stress values are generated at the thread runout, as shown in **Fig. 10.**

The location of the maximum stress in the shaft of the fixing screw is shown in **Fig. 11.**

Fig. 12 shows the stress distribution, where the maximum stress at the above-mentioned location is very clearly visible.

Fig. 13 shows the measured stress distribution

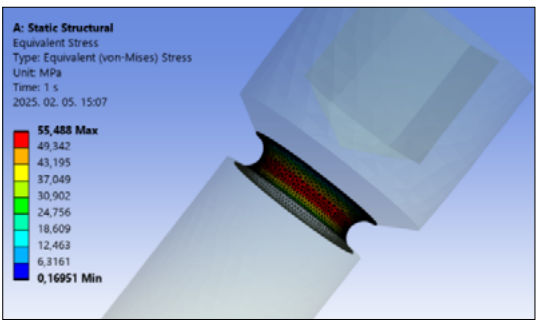

Fig. 10. *Occurring stress at the neck of the screw.*

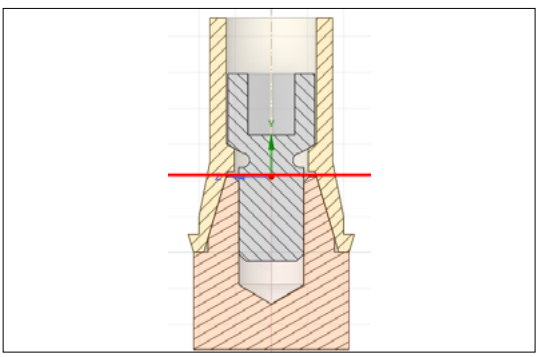

Fig. 11. *Location of the maximum stress within the shaft of the screw.*

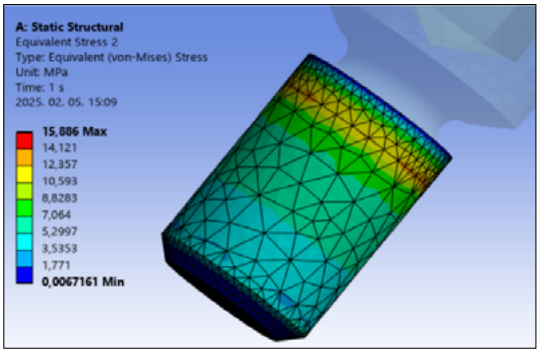

Fig. 12. *Stress distribution in the screw shaft.*

at the screw neck for the fixing screw with 120° vertex angle. In the following diagrams, the horizontal axis of the diagrams shows the different screw tightening torques and the vertical axis shows the maximum stress values in the screw. Each different coloured value (function) corresponds to a different keyhole depth (red dimension in **Fig. 2**).

Fig. 14. shows the stress distribution in the screw shank, measured for a fixing screw with a 120° tip angle.

Fig. 15. shows the measured stress distribution at the screw neck for the fixing screw with 180° vertex angle.

Fig. 16. shows the stress distribution in the screw shank, measured for the fixing screw with a 180° tip angle.

5. Conclusion

As already mentioned in the first chapter, the yield strength of the Ti-6Al-4V ELI material used for the screws is 795 N/mm², based on the manufacturer's catalogue datasheet and the ASTM F136-13 standard, considering the material diameter applied in this study. This means that if the internal stresses arising in the screw reach this value, plastic deformation of the screw will begin. In engineering practice, factors of safety are applied during the design process to reliably prevent such failure.

The chemical composition of the raw material is presented in **Table 1**, while its main mechanical properties are summarized in **Table 2**. These values are taken from the ASTM F136-13 standard, which applies to medical-grade, low-impurity titanium alloys, specifically the wrought and annealed Ti-6Al-4V ELI (Grade 23) titanium alloy. This standard ensures that the material meets the stringent requirements imposed by medical applications **[10]**.

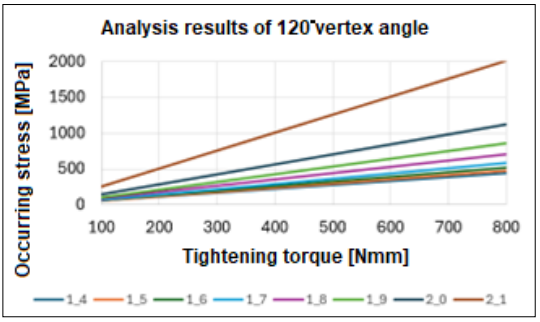

Fig. 13. *Analysis results of 120° vertex angle (at the screw neck).*

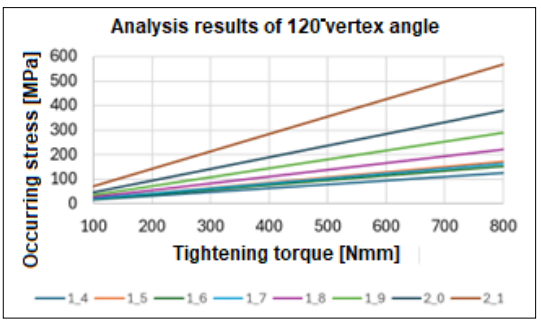

Fig. 14. *Analysis results of 120° vertex angle (within the screw shaft).*

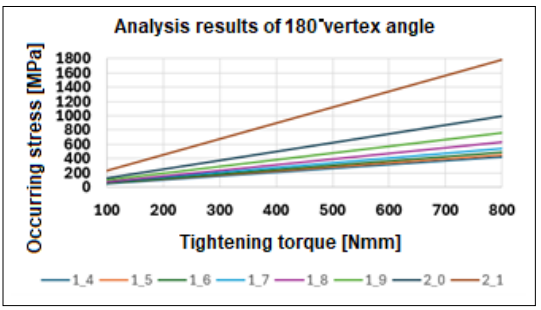

Fig. 15. *Analysis results of 180° vertex angle (at the screw neck).*

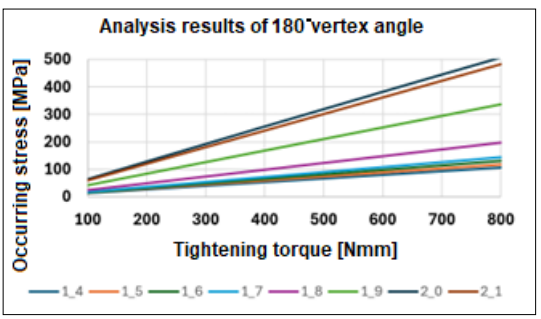

Fig. 16. *Analysis results of 180° vertex angle (within the screw shaft).*

Table 1. *Chemical composition of Ti-6AL-4V-ELI alloy*

Ti-6AL-4V-ELI (ASTM F136) mass %	
Al	5.5–6.5
V	3.5–4.5
Fe	max 0.25
O	max 0.13
C	max 0.08
Ti	rest

Table 2. *Mechanical properties of Ti-6AL-4V-ELI alloy*

Ti-6Al-4V-ELI | (ASTM F136) Mechanical properties	
Density	4.47 g/cm^3
Melting point	1649 °C
Beta transition temperature	977 ± 4 °C
Thermal conductivity (at 20°C)	6.6 W/m°C
Yield strength (at 20°C)	min 795 N/mm^2
Tensile strength (at 20°C)	min 860 N/mm^2
Elongation (at 20°C)	10%

Table 3. *Maximum stress values in the screw in the case of a 120° pilot hole*

Results are shown in N/mm^2 ($\sigma_{120°}$)						
Drill hole length (mm)	Tightening torque (Ncm)					
	25	30	40	50	65	80
1.4	137	165	220	275	357	440
1.5	148	177	236	295	384	472
1.6	163	196	261	326	424	522
1.7	183	220	294	367	477	587
1.8	220	264	352	440	572	704
1.9	269	323	430	538	699	861
2	352	423	564	705	916	1128
2.1	631	757	1009	1261	1639	2018

Table 4. *Maximum stress values in the screw in the case of a 180° pilot hole*

Results are shown in N/mm^2 ($\sigma_{180°}$)						
Drill hole length (mm)	Tightening torque (Ncm)					
	25	30	40	50	65	80
1.4	133	159	212	265	345	424
1.5	141	169	225	282	366	451
1.6	152	182	243	304	395	486
1.7	169	202	270	337	438	540
1.8	198	237	316	396	514	633
1.9	239	287	382	478	621	765
2	310	372	497	621	807	993
2.1	558	670	893	1117	1452	1787

Low impurity content is of paramount importance to achieve good biocompatibility.

When evaluating the results, three different cases and three safety factors are shown. In the first case the factor of safety n = 1. Thus, the maximum allowable internal stress is 795 N/mm^2. Values exceeding this are shown in **Table 3** and **4** on a red background. In the second case the factor of safety is n = 1.5. Thus, the maximum allowable internal stress is 530 N/mm^2 (values exceeding this are shown on an orange background). In the last case, the factor of safety is n = 2,5, in which case the maximum allowed stress value is 318 N/mm^2 (values exceeding this value are marked with a yellow background). In cases where the tables do not show any other colour (white background) for the stress value obtained, there is certainly no failure (calculated with a factor of safety of n = 2,5).

Table 3 shows the maximum stress values for the 120° and **Table 4** for the 180° holes as a function of the inner-wrench-hole depths (**Fig. 1**, size in red) and tightening torques (25-80 Ncm).

The upper limit of the tightening torque range of 25±5 Ncm for screws is 30 Ncm. Based on the simulation results obtained, different maximum pilot hole depth could be determined depending on whether the pilot hole for the internal keyway had a 120° or 180° vertex angle. Based on the maximum stresses, the maximum hole length for the 120° case was 1.8 mm and for the 180° case was 1.9 mm. Both cases considered a safety factor of n = 2.5.

Based on our results and experience, we recommend the use of 180° vertex angle pilot drills in the future, as simulation results show that in this case, by an average of 8.44% lower stress values can be expected. This, in turn, allows longer internal keyhole openings to be produced. The big advantage of a deeper keyhole opening is that a higher tightening torque can be safely achieved when tightening the screws without damaging either the key or the screw.

Table 5. *Percent differences of maximum internal stresses within the screw*

Pilot hole length	Maximum torque difference (Dif)
1.4 mm	3.42%
1.5 mm	4.46%
1.6 mm	6.87%
1.7 mm	8.11%
1.8 mm	10.08%
1.9 mm	11.17%
2 mm	11.93%
2.1 mm	11.45%

Table 5 shows the percentage difference in internal stresses for given hole lengths for the 120° and 180° vertex angle holes. It can be observed that the magnitude of the differenced shows a continuous increase with increasing hole depths. For holes with a depth of 1.9 mm, the deviation is as high as 11.17%.

Formula (1) was used to calculate the values in the table.

$$Dif = 1 - (\sigma_{180°}/\sigma_{120°}) \quad (1)$$

6. Future research opportunities

Avoiding screw breakage when tightening screws during surgery is of paramount importance. If screw failure is clearly detected during surgery (head break-off), the screw must be removed and a new screw must be inserted. Removal of the screw(s) may mean increased surgery time, which may increase anaesthetic complications and thus lead to consequential additional costs. An even more significant problem is when deformation or failure of the screw is not detected and there is no clear external sign of it. This can be the case, for example, when the internal head stresses due to tightening reach the yield point, causing the head of the screw to twist relative to the shank, but no full fracture occurs because the stresses do not reach the tensile strength of the material. In this case, the quality of the connection is inadequate due to damaged screws, which can lead to early implant failure.

For these reasons, we would like to continue our research in the following directions:

- investigation of the stress concentration effects of different thread runout geometries,
- production of physical screws and testing of their failure modes. This would validate our simulation results,
- design and testing of new screw designs (optimisation of head height, internal hole length, head diameter, investigation of the possibility of using self-locking tapered designs to eliminate possible loosening),
- examination of screw materials and their post-processing (heat treatments),
- determination of the optimum tightening torque range for M1.8 and M2 bolts, using both simulation and physical tests.

Acknowledgement

We would like to thank Dent-Art Ltd. for the test pieces (interfaces, screws) provided, and the company's employees, especially Dr. János Kónya, the company's manager, for the consultation opportunities and professional assistance. Their experience and help greatly accelerated the progress of our research.

In addition, special thanks to Abricad Ltd. for temporarily providing us with access to their SolidWorks design software. This allowed us to create 3D models of the screw and the interface.

Additionally, we would like to thank the Ministry of Culture and Innovation and the National Research, Development and Innovation Fund for their support under the University Research Fellowship Program (EKÖP-KDP), which has been awarded to Ádám Vörös. This was a great help both during the research and during the writing of the article.

References

[1] Stein E.: *History of the Finite Element Method – Mathematics Meets Mechanics – Part I: Engineering Developments.* In: The History of Theoretical, Material and Computational Mechanics – Mathematics Meets Mechanics and Engineering. (Editor: Stein E.). Springer Berlin, Heidelberg, 2013. 399–442.

[2] Dolgov V. Y., Klyshnikov K. Y., Ovcharenko E. A., Glushkova T. V., Batranin A. V., Agienko A. S., et al.: *Finite Element Analysis-Based Approach for Prediction of Aneurysm-Prone Arterial Segments*. Journal of Medical and Biological Engineering, 39/1. (2019) 102–108. https://doi.org/10.1007/s40846-018-0422-x

[3] Gizzi A., De Bellis M. L., Vasta M., Pandolfi A.: *Diffusion-Based Degeneration of the Collagen Reinforcement in the Pathologic Human Cornea.* Journal of Engineering Mathematics, 127/3. (2021) 1–27. https://doi.org/10.1007/s10665-020-10088-x

[4] Heller M. O.: *Finite Element Analysis in Orthopedic Biomechanics.* In: Human Orthopaedic Biomechanics. (Innocenti B. and Galbusera F.) Academic Press, Southampton, 2022. 637–658.

[5] Geng J., Tan K. B. C., Liu G.: *Application of Finite Element Analysis in Implant Dentistry: a Review of*

the Literature. The Journal of Prosthetic Dentistry, 85/6. (2001) 585–598. https://doi.org/10.1067/mpr.2001.115251

[6] Alkan I., Sertgöz A., Ekici B.: *Influence of Occlusal Forces on Stress Distribution in Preloaded Dental Implant Screws*. The Journal of Prosthet Dentistry, 91/4. (2004) 319–325. https://doi.org/10.1016/j.prosdent.2004.01.016

[7] Assenza B., Scarano A., Leghissa G., Carusi G., Thams U., Roman F.S., Piattelli A.: *Screw- Vs Cement-Implant-Retained Restorations: an Experimental Study in the Beagle. Part 1. Screw and Abutment Loosening*. Journal of Oral Implantology, 31/5. (2005) 242–246. https://doi.org/10.1563/1548-1336(2005)31[242:SVCRAE]2.0.CO;2

[8] Pjetursson B. E., Thoma D., Jung R., Zwahlen M., Zembic A.: *A Systematic Review of the Survival and Complication Rates of Implant-Supported Fixed Dental Prostheses (FDPs) After a Mean Observation Period of at Least 5 Years*. Clinical Oral Implants Research, 23/6. (2012) 22–38. https://doi.org/10.1111/j.1600-0501.2012.02546.x

[9] Jaber H., Kónya J., Kulcsár K., Kovács T.: *Effects of Annealing and Solution Treatments on the Microstructure and Mechanical Properties of Ti6Al4V Manufactured by Selective Laser Melting*. Materials, 15/5. (2022) https://doi.org/10.3390/ma15051978

[10] ASTM F136: Titanium Alloys. Standard Specification for Wrought Titanium-6Aluminum-4Vanadium ELI (Extra Low Interstitial) Alloy for Surgical Implant